Letter

Low-dimensional dynamics of globally coupled complex Riccati equations: Exact firing-rate equations for spiking neurons with clustered substructure

Diego Pazó [1] and Rok Cestnik [2]

[1] *Instituto de Física de Cantabria (IFCA), Universidad de Cantabria-CSIC, 39005 Santander, Spain*

[2] *Centre for Mathematical Science, Lund University, 22100 Lund, Sweden*

(Received 30 October 2024; revised 4 March 2025; accepted 18 April 2025; published 12 May 2025)

We report on an exact theory for ensembles of globally coupled, heterogeneous complex Riccati equations. A drastic dimensionality reduction to a few ordinary differential equations is achieved for Lorentzian heterogeneity. By applying this technique, we obtain low-dimensional firing-rate equations for populations of spiking neurons with a clustered substructure.

DOI: 10.1103/PhysRevE.111.L052201

Introduction. Dimensionality reduction methods are of paramount importance in physics. Keeping only the essential degrees of freedom improves our insight into the system behavior and increases our chances of controlling it. Standard dimensionality reduction techniques are approximate. Remarkably, years ago, Ott and Antonsen [1] discovered an ansatz which permitted an exact dimensionality reduction to a few ordinary differential equations (ODEs) for populations of heterogeneous phase oscillators. This method was profusely applied to Kuramoto-like models, and pulse-coupled oscillators [2,3], greatly improving our understanding of them [4]. Subsequently, a close relative of the Ott-Antonsen ansatz, the so-called Lorentzian ansatz, made it possible to derive low-dimensional closed equations for ensembles of spiking neurons of quadratic integrate-and-fire (QIF) type [5]. The Lorentzian ansatz was key for deriving exact firing-rate equations (FREs) [5], i.e., for establishing a theoretical link between ensembles of individual neurons and mesoscopic firing-rate (or neural-mass) dynamics. In subsequent years, many variants and extensions of this methodology appeared, see, e.g., Refs. [6–16]. This framework, known as next-generation neural-mass models [17,18], was also used in practical and clinical studies in neuroscience [19,20].

Exact dimensionality reduction appeared to be limited to ensembles of one-dimensional units (phase models or QIF neurons). However, a generalization of the Ott-Antonsen ansatz for orientable agents on a D-dimensional sphere recently appeared [21]. More recently, one of us found that, like in certain arrays of phase oscillators [22], arrays of identical complex-valued Riccati equations are quasi-integrable [23]. Interestingly, the complex Riccati equation, a planar nonlinear system, appears at an intermediate step in the derivation of the FREs mentioned above as well as in calculations with the Ott-Antonsen ansatz. Therefore, developing a specific dimensionality reduction scheme for ensembles of heterogeneous Riccati equations widens the scope of solvable ensembles in a nontrivial way.

In this letter, we present a dimensionality reduction scheme for ensembles of heterogeneous Riccati equations. The power of this method is exemplified by obtaining exact low-dimensional FREs for ensembles of QIF neurons with a clustered substructure. Numerical simulations confirm the validity of our approach.

Complex-valued Riccati ODEs. We study ensembles of heterogeneous complex-valued Riccati ODEs

$$\dot{z}_j = a_j z_j^2 + b_j z_j + c_j, \tag{1}$$

where $z_j(t) \in \mathbb{C}$, and index j runs from 1 to the population size $N \gg 1$. Equation (1) contains three complex coefficients: a_j, b_j, and c_j, which depend on the complex mean field

$$Z(t) = \frac{1}{N}\sum_{j=1}^{N} z_j. \tag{2}$$

(Explicit dependence on time is also possible.) The coefficients (a_j, b_j, c_j) vary across units, as indicated by the index j. Heterogeneity is introduced via (scalar or vector) parameters $\boldsymbol{\eta}_j$, which are drawn from a continuous probability density function (PDF) $G(\boldsymbol{\eta})$. Hence, $a_j = a(\boldsymbol{\eta}_j, Z, t)$, likewise for b_j and c_j.

Ansatz for the thermodynamic limit. Our theoretical analysis adopts the thermodynamic limit ($N \to \infty$). We define a conditional density $\rho(z, \bar{z}|\boldsymbol{\eta}; t)$, which satisfies the continuity equation (expressed with complex variables):

$$\partial_t \rho + \partial_z(\rho \dot{z}) + \partial_{\bar{z}}(\rho \dot{\bar{z}}) = 0, \tag{3}$$

where $\bar{z}$ stands for the complex conjugate of z. We here present the following ansatz as an exact solution of the continuity equation:

$$\rho(z, \bar{z}|\boldsymbol{\eta}; t) = \frac{\alpha(\boldsymbol{\eta}, t)^2}{\pi[|z - q(\boldsymbol{\eta}, t)|^2 + \alpha(\boldsymbol{\eta}, t)^2]^2}. \tag{4}$$

This density is bell shaped, with its center located at $q \in \mathbb{C}$ and radial width $\langle |z - q| \rangle = (\pi/2)\alpha \geqslant 0$.

The form of Eq. (4) was suggested by the stereographic projection of a uniform density on the surface of the unit three-dimensional (3D) sphere onto the complex plane, with an offset q and a width α as free parameters. Originally, the motivation for this stems from the mapping between the dynamics of an orientable agent on a 3D sphere and the

Riccati dynamics with real coefficients, see Ref. [24] for illustration.

The functional form of the density in Eq. (4) is invariant under time evolution, with q and α obeying

$$\partial_t q(\boldsymbol{\eta}, t) = aq^2 + bq + c - \bar{a}\alpha^2, \tag{5a}$$

$$\partial_t \alpha(\boldsymbol{\eta}, t) = [aq + \bar{a}\bar{q} + (b + \bar{b})/2]\alpha. \tag{5b}$$

Closing this system of equations requires determining the mean field. For a given $\boldsymbol{\eta}$ value, the average is located at $q(\boldsymbol{\eta}, t)$, and the continuous counterpart of Eq. (2) is obtained by integrating q over $\boldsymbol{\eta}$:

$$Z(t) = \int G(\boldsymbol{\eta})\, q(\boldsymbol{\eta}, t)\, d\boldsymbol{\eta}. \tag{6}$$

Equations (5) and (6) define a closed system of integrodifferential equations, which exactly governs the dynamics in the subspace determined by our density ansatz in Eq. (4).

Reduction to ODEs. Further reduction to ODEs is possible in certain cases only. We focus hereafter on one of these cases. From now on, only the real part of c_j is heterogeneous:

$$a_j = a(Z, t), \tag{7a}$$

$$b_j = b(Z, t), \tag{7b}$$

$$c_j = \eta_j + i\,\Gamma + f(Z, t), \tag{7c}$$

where η_j and Γ are real, and $f = f_r + i f_i$ is a complex function. Hence, in the $N \to \infty$ limit, the mean field is obtained by integrating over the only source of heterogeneity

$$Z(t) = \int_{-\infty}^{\infty} g(\eta)\, q(\eta, t)\, d\eta, \tag{8}$$

where $g(\eta)$ is the PDF of η.

A particularly sharp reduction of dimensionality is achieved for a Lorentzian distribution of the heterogeneity $\eta_j \sim L(\eta_j|\eta_0, \delta)$:

$$g(\eta) = L(\eta|\eta_0, \delta) = \frac{\delta/\pi}{(\eta - \eta_0)^2 + \delta^2}. \tag{9}$$

Here, η_0 is the center of the distribution, and $\delta > 0$ denotes its half-width at half-maximum (HWHM). We can evaluate the integral in Eq. (8) using the residue theorem. By closing the integration path with an arc at complex infinity, the integral takes the value of $q(\eta_p, t)$, where η_p is the pole of $g(\eta) = (2\pi i)^{-1}[(\eta - \eta_0 - i\delta)^{-1} - (\eta - \eta_0 + i\delta)^{-1}]$ located inside the integration contour—provided q is analytic inside. The suitable pole turns out to be [25]

$$\eta_p = \eta_0 \pm i\delta, \quad \text{with} \quad \pm = \operatorname{sgn}\left(\Gamma + f_i - \frac{b_r b_i}{2a}\right), \tag{10}$$

with $b = b_r + i\, b_i$ and assuming real $a > 0$. In this way, the mean field in Eq. (8) becomes

$$Z(t) = q(\eta_p, t). \tag{11}$$

Evaluating Eq. (5) at η_p dramatically reduces the dimensionality of the problem. For closing this system of ODEs, we must also evaluate the variable $\bar{q}$ at the pole η_p. Noting that $\bar{q}(\eta, t)$ is governed by Eq. (5a) under complex conjugation, we end up with a system of three complex-valued ODEs for variables $\{Z, A, Q\} = \{q, \alpha, \bar{q}\}_{\eta=\eta_p}$:

$$\dot{Z} = aZ^2 + bZ + \eta_p + i\Gamma + f - aA^2, \tag{12a}$$

$$\dot{A} = [a(Z + Q) + (b + \bar{b})/2]A, \tag{12b}$$

$$\dot{Q} = aQ^2 + \bar{b}Q + \eta_p - i\Gamma + \bar{f} - aA^2. \tag{12c}$$

This system describes the dynamics of an infinite ensemble of Riccati equations inside the manifold defined by densities of the form in Eq. (4). Next, we showcase the reduced Eq. (12) on a physically meaningful example.

FREs for clustered neurons. Firing-rate models constitute useful representations of the activity of ensembles of neurons in terms of a few collective variables [18,26]. A decade ago, an exact reduction to a system of two ODEs was achieved for ensembles of globally coupled QIF neurons [5].

Here, we go one step further and consider a population consisting of N subpopulations of internally coupled QIF neurons. The microscopic equations are

$$\dot{V}_{i,j} = V_{i,j}^2 + \eta_{i,j} + \phi(r_j) + f(R, t), \tag{13}$$

$$r_j = \frac{1}{M}\sum_{i=1}^{M}\sum_k \delta^{(\epsilon)}\big(t - t_{i,j}^k\big), \tag{14}$$

$$R = \frac{1}{N}\sum_{j=1}^{N} r_j. \tag{15}$$

Here, $V_{i,j}(t) \in \mathbb{R}$ is the membrane potential of the ith neuron in the jth subpopulation. The $\delta^{(\epsilon)}$ function in Eq. (14) represents the spikes at firing times $t_{i,j}^k$ (when $V_{i,j}$ reaches ∞ and is reset to $-\infty$) and becomes the Dirac delta after taking $M \to \infty$. The r_j's are average firing rates of subpopulations, while R is the global firing rate. The internal coupling in each subpopulation is represented by the function $\phi(r_j)$, while the coupling f in Eq. (13) is the result of every QIF neuron interacting with all the other ones at the global scale.

In the $M \to \infty$ limit, for Lorentzian distributed internal currents $\eta_{i,j} \sim L(\eta_{i,j}|\eta_j, \Delta)$, applying the method in Ref. [5] yields an ensemble of globally coupled FREs. The state of each node is given by the firing rate r_j and the membrane voltage $v_j = M^{-1}\ \sum_i V_{i,j}$. Their evolution is governed by ODEs

$$\dot{v}_j = v_j^2 - \pi^2 r_j^2 + \eta_j + \phi(r_j) + f(R, t), \tag{16a}$$

$$\dot{r}_j = 2v_j r_j + \frac{\Delta}{\pi}. \tag{16b}$$

Recall that parameters η_j and $\Delta > 0$ are the center and the HWHM of the Lorentzian distribution of internal currents $\eta_{i,j}$ in the jth subpopulation of QIF neurons [5]. More generally, Δ can represent the sum of the HWHM and the amplitude of Cauchy noise [15,16]. The main variables and parameters are summarized in Table I.

For physical reasons, ϕ must be a monotonic function with $\phi(0) = 0$. For solvability, we choose the quadratic function $\phi(r) = \kappa\, r^2$. This is different from the standard linear function but can be used to approximate a linear interaction around a reference firing rate r_0: $r \approx r^2/(2r_0) - r_0/2$, or it can appear from triplet interactions. The constant κ represents inhibitory coupling for $\kappa < 0$ and excitatory coupling for $\kappa > 0$.

TABLE I. Variables and internal parameters at each description level for the two examples of dimensionality reduction in this letter. $L(h|h_0, d)$ indicates h is Lorentzian distributed with center at h_0 and HWHM d. Coupling parameters depend on the specific example and are not included here.

	Voltages	Rates	Internal parameters
Neurons	$V_{i,j}$	—	$\eta_{i,j} \sim L(\eta_{i,j}\|\eta_j, \Delta)$
Subpopulations	v_j	r_j	Δ and $\eta_j \sim L(\eta_j\|\eta_0, \delta)$
Whole population	V	R	δ and η_0

For $\kappa < \pi^2$, we can define the complex variable

$$z_j \equiv v_j + i(\pi^2 - \kappa)^{1/2} r_j, \tag{17}$$

such that Eq. (16) becomes an ensemble of globally coupled Riccati equations

$$\dot{z}_j = z_j^2 + \eta_j + i(1 - \kappa/\pi^2)^{1/2}\Delta + f(R, t). \tag{18}$$

We adopt the standard chemical coupling $f = JR$, where J is the coupling constant, and $R = \mathrm{Im}(Z)/(\pi^2 - \kappa)^{1/2}$. In Fig. 1, we show the result of simulating an ensemble of 10^4 units with Lorentzian distributed η_j and an initial condition $z_j(0)$ drawn randomly from the density in Eq. (4) with η-independent parameters $q(\eta, 0) = q_0$ and $\alpha(\eta, 0) = \alpha_0$. The two panels in Fig. 1 differ only in the value of α_0: 0.5 and 2 for (a) and (b), respectively. It may be appreciated that the average Z behaves in very good agreement with the prediction of the corresponding six-dimensional model in Eq. (12). The conformity between the simulation and the theory is remarkable, especially considering that the two different initial conditions lead to distinct attractors.

For the system in Eq. (18), A always approaches zero asymptotically. This follows from the coincidence (up to a factor 6) between the real part of the coefficient accompanying A in Eq. (12b) and the trace of the Jacobian of the system $6[a\mathrm{Re}(Z + Q) + b_r]$, which determines the volume contraction rate and is negative on average [27] (unless the system is conservative). This means that the asymptotic behaviors of the system are well described by Eq. (12a) alone, setting $A = 0$. One could have derived that equation assuming from the outset that there is a (smooth) univocal dependence of z_j on the value of η_j (i.e., $\alpha = 0$). This assumption enables the transformation $z_j(t) \to z(\eta, t)$ and immediately leads to Eq. (5a) with $\alpha = 0$.

It is instructive to revert the change of variables defined in Eq. (17) and write down the equation for the asymptotic dynamics of mean voltage $V = N^{-1}\sum_j v_j$ and firing rate R:

$$\dot{V} = V^2 - (\pi^2 - \kappa)R^2 + \eta_0 + JR, \tag{19a}$$

$$\dot{R} = 2VR + \frac{\Delta}{\pi} + \frac{\delta}{(\pi^2 - \kappa)^{1/2}}. \tag{19b}$$

These two ODEs exactly describe the asymptotic global behavior of an ensemble of QIF neurons with two levels of heterogeneity and coupling. The microscopic level depends on parameters Δ and κ, while at the mesoscopic level, δ and J play that role. The phase diagram of the system in Eq. (19) is trivial since the FREs in Ref. [5] are recovered, after appropriate rescaling of R, and defining effective J and Δ parameters. For $\kappa = 0$, we consistently recover the FREs for Lorentzian heterogeneity of currents centered at η_0 and HWHM $\Delta + \delta$ [28].

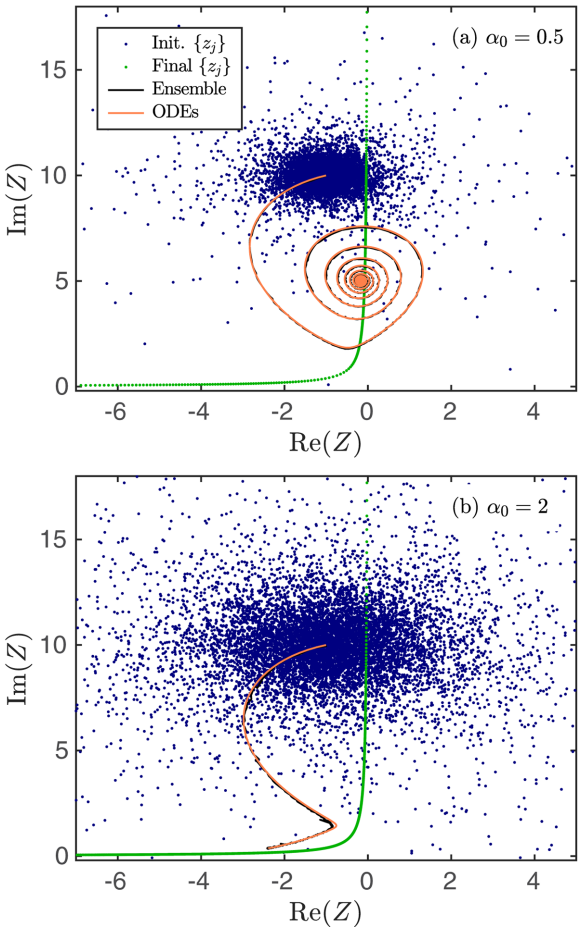

FIG. 1. Phase portraits of the mean field Z for two different initial conditions. The black line is the trajectory of Z obtained by simulating an ensemble of 10^4 units, while the orange line shows the prediction from the reduced model of three complex-valued ordinary differential equations (ODEs), Eq. (12). System parameters are $\kappa = \pi^2/2$, $J = 16$, $\eta_0 = -8$, and $\Delta = \delta = 1$. Initial conditions were chosen according to the ansatz in Eq. (4) with $q_0 = -1 + 10i$, and the only difference between the two panels is the width of the initial distribution α_0, set to 0.5 in (a) and 2 in (b). The initial and final states of the ensemble of units $\{z_j\}_{j=1,\ldots,N}$ are depicted with blue and green dots, respectively. Animations of the figures are available in the Supplemental Material [30].

Global electrical coupling. The synapses between neurons can be either chemical or electrical (gap junctions). Electrical coupling may trigger unsteady periodic dynamics in one single population of QIF neurons without additional ingredients such as delay [10]. Hence, we modify our ensemble of QIF neurons considering a global electrical coupling instead of chemical coupling. The form of the internal coupling $\phi(r_j)$ is preserved. The ensemble of FREs turns out to obey [29]

$$\dot{v}_j = v_j^2 - (\pi^2 - \kappa)r_j^2 + \eta_j + g(V - v_j), \tag{20a}$$

$$\dot{r}_j = 2v_j r_j + \frac{\Delta}{\pi} - g r_j. \tag{20b}$$

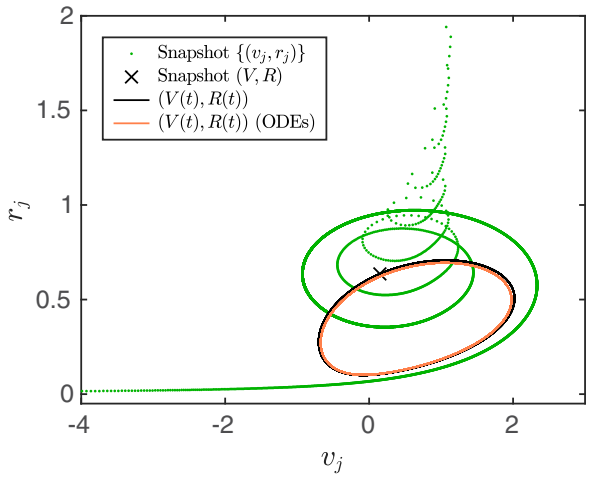

FIG. 2. Snapshot of the coordinates of system in Eq. (20) with $N = 8000$ in its asymptotic regime, see green dots. The location of the mean field is signaled by a $\times$. The trajectory of the mean field $[V(t), R(t)]$ extracted from the direct simulation of Eq. (20) and the limit cycle predicted by Eq. (21) are depicted by black and orange solid lines, respectively. Parameters: $g = 2.5$, $\kappa = -\pi^2$, $\eta_0 = 1$, and $\Delta = \delta = 0.5$.

Now the global coupling actuates through the mean voltage $V(t)$, and $g > 0$ is the conductance. A global chemical coupling term $J R$ could also be included, but we opted not to do so for simplicity.

We apply the transformation in Eq. (17) and our reduction theory to Eq. (20). If we exclusively focus on the asymptotic dynamics, we need only the complex-valued ODE in Eq. (12a) with $A = 0$. Written in terms of V and R, it yields exact macroscopic FREs

$$\dot{V} = V^2 - (\pi^2 - \kappa)R^2 + \eta_0, \tag{21a}$$

$$\dot{R} = 2VR + \frac{\Delta}{\pi} + \frac{\delta}{(\pi^2 - \kappa)^{1/2}} - gR. \tag{21b}$$

We test the validity of these FREs combining global electrical coupling with inhibitory internal coupling ($\kappa < 0$) in each subpopulation. Figure 2 shows the comparison between the oscillatory behavior of the ensemble in Eq. (20) and the limit cycle displayed by the system of ODEs in Eq. (21). Again, we find very good agreement between theory and simulation.

Conclusions. In this letter, we have uncovered an exact dimensionality reduction scheme for an infinite set of globally coupled complex-valued Riccati equations. Our approach begins with an ansatz for the continuity equation, which defines a lower-dimensional manifold. The application of the residue theorem further reduced the dimensionality to only three complex-valued ODEs, Eq. (12). The mathematical analysis assumed that, if an initial $q(\eta, 0)$ possesses an analytic continuation in a particular complex η half-plane, it remains analytic under time evolution. This might not be completely justified since $\bar{q}(\eta, t)$ does not remain analytic in the same half-plane, and it drives q via α. This limitation raises the question of whether the six-dimensional system in Eq. (12) is merely an excellent approximation. In the large-time limit, $A(t)$ almost always approaches 0, and the resulting asymptotic two-dimensional system exactly describes the attractors (in the thermodynamic limit).

We applied our theory to ensembles of FREs, confirming the validity of our approach. All simulations showed good agreement with the theory. The reduced six-dimensional model consistently predicted the correct asymptotic states across initial conditions, despite the analyticity issue discussed above. Moreover, the two-dimensional systems in Eqs. (19) and (21) perfectly described the attractors.

It is noteworthy that, with this formalism, one could consider arbitrarily nested substructures since, at each step, the equations can be of the Riccati form given a certain form of coupling, e.g., for $f = J R^2$, Eq. (19) is equivalent to a Riccati equation [30].

Our methodology represents a significant breakthrough in dimensional reductions, as it expands the solvable examples from traditional one-dimensional units into the realm of planar units. This opens up many examples to explore, with many unit and coupling dynamics one can choose from. Additionally, the heterogeneity may enter in several ways (not only in the real part of c_j). Beyond the variations to the FREs that were studied here, we can also mention the complexified Kuramoto model [31,32] as a system where our methodology can be applied.

Acknowledgments. D.P. acknowledges support by Grant No. PID2021-125543NB-I00, funded by MICIU/AEI/10.13039/501100011033 and by ERDF/EU. R.C. acknowledges financial support from the Royal Swedish Physiographic Society of Lund.

Data availability. The data that support the findings in this paper are not publicly available. The data are available from the authors upon reasonable request.

[1] E. Ott and T. M. Antonsen, Low dimensional behavior of large systems of globally coupled oscillators, Chaos **18**, 037113 (2008).

[2] T. B. Luke, E. Barreto, and P. So, Complete classification of the macroscopic behavior of a heterogeneous network of theta neurons, Neural Comput. **25**, 3207 (2013).

[3] D. Pazó and E. Montbrió, Low-dimensional dynamics of populations of pulse-coupled oscillators, Phys. Rev. X **4**, 011009 (2014).

[4] C. Bick, M. Goodfellow, C. R. Laing, and E. A. Martens, Understanding the dynamics of biological and neural oscillator networks through exact mean-field reductions: a review, J. Math. Neurosci. **10**, 9 (2020).

[5] E. Montbrió, D. Pazó, and A. Roxin, Macroscopic description for networks of spiking neurons, Phys. Rev. X **5**, 021028 (2015).

[6] D. Pazó and E. Montbrió, From quasiperiodic partial synchronization to collective chaos in populations of inhibitory neurons with delay, Phys. Rev. Lett. **116**, 238101 (2016).

[7] I. Ratas and K. Pyragas, Macroscopic self-oscillations and aging transition in a network of synaptically coupled quadratic integrate-and-fire neurons, Phys. Rev. E **94**, 032215 (2016).

[8] F. Devalle, A. Roxin, and E. Montbrió, Firing rate equations require a spike synchrony mechanism to correctly describe fast oscillations in inhibitory networks, PLoS Comput. Biol. **13**, e1005881 (2017).

[9] M. di Volo and A. Torcini, Transition from asynchronous to oscillatory dynamics in balanced spiking networks with instantaneous synapses, Phys. Rev. Lett. **121**, 128301 (2018).

[10] B. Pietras, F. Devalle, A. Roxin, A. Daffertshofer, and E. Montbrió, Exact firing rate model reveals the differential effects of chemical versus electrical synapses in spiking networks, Phys. Rev. E **100**, 042412 (2019).

[11] E. Montbrió and D. Pazó, Exact mean-field theory explains the dual role of electrical synapses in collective synchronization, Phys. Rev. Lett. **125**, 248101 (2020).

[12] R. Gast, H. Schmidt, and T. R. Knoesche, A mean-field description of bursting dynamics in spiking neural networks with short-term adaptation, Neural Comput. **32**, 1615 (2020).

[13] D. S. Goldobin, M. di Volo, and A. Torcini, Reduction methodology for fluctuation driven population dynamics, Phys. Rev. Lett. **127**, 038301 (2021).

[14] L. Chen and S. A. Campbell, Exact mean-field models for spiking neural networks with adaptation, J. Comput. Neurosci. **50**, 445 (2022).

[15] B. Pietras, R. Cestnik, and A. Pikovsky, Exact finite-dimensional description for networks of globally coupled spiking neurons, Phys. Rev. E **107**, 024315 (2023).

[16] P. Clusella and E. Montbrió, Exact low-dimensional description for fast neural oscillations with low firing rates, Phys. Rev. E **109**, 014229 (2024).

[17] S. Coombes and Á. Byrne, Next generation neural mass models, in *Nonlinear Dynamics in Computational Neuroscience*, edited by F. Corinto and A. Torcini (Springer International Publishing, Cham, 2019), pp. 1–16.

[18] S. Coombes and K. C. A. Wedgwood, *Neurodynamics: An Applied Mathematics Perspective* (Springer Nature, Cham, 2023), Vol. 75.

[19] G. Rabuffo, J. Fousek, C. Bernard, and V. Jirsa, Neuronal cascades shape whole-brain functional dynamics at rest, eNeuro **8** (2021).

[20] M. Gerster, H. Taher, A. Škoch, J. Hlinka, M. Guye, F. Bartolomei, V. Jirsa, A. Zakharova, and S. Olmi, Patient-specific network connectivity combined with a next generation neural mass model to test clinical hypothesis of seizure propagation, Front. Syst. Neurosci. **15**, 675272 (2021).

[21] S. Chandra, M. Girvan, and E. Ott, Complexity reduction ansatz for systems of interacting orientable agents: Beyond the Kuramoto model, Chaos **29**, 053107 (2019).

[22] S. Watanabe and S. H. Strogatz, Integrability of a globally coupled oscillator array, Phys. Rev. Lett. **70**, 2391 (1993).

[23] R. Cestnik and E. A. Martens, Integrability of a globally coupled complex Riccati array: Quadratic integrate-and-fire neurons, phase oscillators, and all in between, Phys. Rev. Lett. **132**, 057201 (2024).

[24] D. Pazó, Quasi-integrable arrays: The family grows, Physics **17**, 12 (2024).

[25] If the sign of $\Gamma + f_i - b_r b_i/(2a)$ changes under the time evolution, then our approach breaks down (one cannot simply flip the sign of the $\pm$). Fortunately, that does not occur in many situations. See Supplemental Material [30] for details.

[26] G. B. Ermentrout and D. H. Terman, *Mathematical Foundations of Neuroscience* (Springer, New York, 2010), Vol. 64.

[27] A. Pikovsky and A. Politi, *Lyapunov Exponents* (Cambridge University Press, Cambridge, 2016).

[28] This is precisely the marginal distribution for a conditional Lorentzian distribution $L(\eta|\eta_c, \Delta)$ centered at η_c with HWHM Δ, if η_c is itself Lorentzian-distributed with center η_0 and HWHM δ: $\int d\eta_c L(\eta|\eta_c, \Delta) L(\eta_c|\eta_0, \delta) = L(\eta|\eta_0, \delta + \Delta)$.

[29] The microscopic model of QIF neurons leading to Eq. (20), via Refs. [10,11], is available in the Supplemental Material [30].

[30] See Supplemental Material at http://link.aps.org/supplemental/10.1103/PhysRevE.111.L052201 for additional details and three animations.

[31] M. Thümler, S. G. M. Srinivas, M. Schröder, and M. Timme, Synchrony for weak coupling in the complexified Kuramoto model, Phys. Rev. Lett. **130**, 187201 (2023).

[32] S. Lee, L. Braun, F. Bönisch, M. Schröder, M. Thümler, and M. Timme, Complexified synchrony, Chaos **34**, 053141 (2024).